Generation of terahertz acoustic waves in semiconductor quantum dots using femtosecond laser pulses

P.-A. Mante, A. Devos,* and A. Le Louarn
Institut d'Électronique, de Microélectronique et de Nanotechnologie, Unité Mixte de Recherche CNRS 8250, Avenue Poincaré BP 69, F-59652 Villeneuve d'Ascq Cedex, France
(Received 12 February 2010; published 19 March 2010)

We present experimental results demonstrating that the generation of terahertz acoustic waves using femtosecond laser pulses is possible in quantum dots (QDs). Very short and strong pulses are emitted from a buried QD layer and detected at the sample surface. By tuning the laser wavelength we can detect, at room temperature, frequencies above 1 THz using a photoelastic mechanism. A theoretical model supports such a capability and shows that around an interband transition the bandwidth of the photoelastic detection can be greatly improved. These results suggest that QD can be an ultrahigh-frequency acoustic transducer needed for nanoscale acoustics.

DOI: 10.1103/PhysRevB.81.113305 PACS number(s): 78.47.J−, 43.35.+d, 78.20.hb, 78.67.Hc

With size reduction, more and more mechanical investigations at nanoscale are needed as well as for probing elastic properties or the environment effect on nanoscale objects or interfaces.[1,2] The frequency range which suits very well such a size scale starts from 100 GHz up to a few terahertz. Several experimental techniques permit to study such acoustic phonons, as well in the frequency domain such as Raman or Brillouin light scattering, as in the time domain with ultrafast acoustics. In ultrafast acoustics also known as picosecond acoustics, one uses femtosecond laser pulses to generate and to detect acoustic phonons. A few studies have demonstrated the opportunity to detect subterahertz acoustic waves with such a setup in some specific samples.[3] Concerning generation, a transducer able to emit terahertz acoustic pulses is still needed. In most cases, the generation is made by optical absorption within a thin metallic film. Doing that it is possible to reach frequency up to 300 GHz.[4] New transducers must be developed to reach higher frequencies, and in order to compensate sound attenuation they must be very efficient. Recently, superlattices have been attracting much interest,[5–8] and frequency in the terahertz range has been observed at low temperature.

Previously one of us has shown that QD can be a very efficient phonon emitter.[9] Using a two-color pump-probe experiment, it has been shown that the pump femtosecond light pulse produces a huge phonon emission within the QD layer. The spectral content of such a pulse is expected to reach terahertz frequencies due to small size of the emitting region. Roughly, the central frequency of a phonon wave packet emitted from a region which size is ζ is given by v/ζ, where v is the longitudinal sound velocity. Assuming a 3-nm-height InAs QD layer and a sound velocity of 3.83 $\mathrm{nm.ps}^{-1}$, we expect the central frequency to fall in the terahertz range.[10] Unfortunately, in these previous experiments the phonon wave packets were detected at the free surface by the photoelastic mechanism which was limited to 100 GHz.[9] So the question of frequency content of the huge acoustic pulses emitted from QD is still open.

In this Brief Report, we present experimental results which confirm the high-frequency content of the acoustic pulse emitted from the QD layer. By playing on the experimental conditions, we are able to detect frequency above 1 THz at room temperature. Such a high-frequency component is detected by means of the photoelastic mechanism and some specific experimental condition. A theoretical model supports these results, and experimental signals are reproduced using a numerical modeling.

Experiments were performed on epitaxially grown InAs quantum dots buried in InP.[11] Two samples with different cap thickness, each containing one layer of InAs QD, were studied. The nominal thicknesses of the cap are 400 and 100 nm and the InP substrate orientation is (311). The time-resolved experiments are carried on using a tunable Ti:sapphire oscillator and a conventional two-color pump and probe setup at normal incidence. The laser produces 120 fs optical pulses at a repetition rate of 80 MHz, centered at a wavelength tunable between 690 and 1040 nm. Figure 1(a) presents a schematic diagram of the experimental setup. We used an infrared

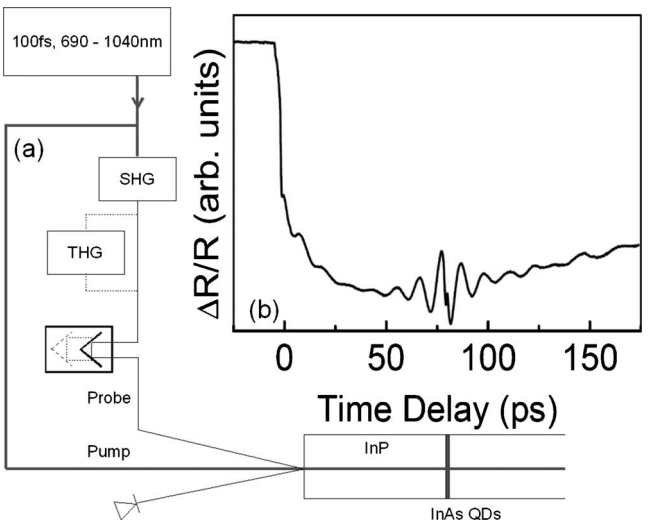

FIG. 1. (a) Schematic diagram of the experimental setup. SHG = second-harmonic generator. THG = third-harmonic generator. The infrared pump penetrates deeply inside the sample, whereas the blue or UV probe is absorbed at the sample surface. (b) Experimental signal obtained on the 400-nm-thick cap sample at a probe wavelength of 450 nm.

pump while the probe is either frequency doubled or frequency tripled.[12] As explained in the following, we need to reach lower wavelengths for probing the high-frequency content of the acoustic pulse. For that, we realized a third-harmonic generator to obtain a UV probe from the near infrared output of the laser. Following previous work, frequency tripling is made as a cascaded process; first the laser is frequency doubled by focusing the input beam in a 1-mm-thick LiB_3O_5 (LBO) crystal. LBO is preferred to β-BaB_2O_4 (BBO) to ensure a good spatial profile. Then the third harmonic is obtained by a subsequent sum frequency generation using type I phase matching in a 0.5-mm-thick BBO crystal.[13] All the experiments are performed at room temperature.

Figure 1(b) shows the transient reflectivity obtained at a probe wavelength of 450 nm on the sample with a 400-nm-thick cap. One first remarks an initial drop of the reflectivity produced by photogenerated carriers on an ultrafast time scale. It is followed by a slow increase due to electronically and thermally induced variation of the refractive index. Another strong structure appears around 80 ps, it corresponds to the arrival of the acoustic phonon wave packet generated within the buried QD layer. As described in details in Ref. 9, two strain pulses are emitted from the pump light pulse: one from the free surface and one from the QD layer. Both are detected at the free surface by the blue probe which penetrates the cap only from a few nanometers. The detection of the first pulse is visible in the first picoseconds as an oscillating part. On the other hand, the pulse coming from the QD layer is detected at a delay which exactly corresponds to the time needed for a longitudinal-acoustic wave to go across the cap. The oscillating part of the echo detection is an evidence of the photoelastic nature of the detection mechanism. Indeed, such oscillations so-called Brillouin oscillations result from interferences between the probe light reflected at interfaces and the one reflected by the acoustic pulse.[14] The frequency is given by $f=2nv/\lambda$ where n is the refractive index, v is the longitudinal sound velocity and λ the probe wavelength.[14] In case of InP, the frequency detected using a 450 nm probe is close to 100 GHz. In other words, the detection of the pulse coming from the QD is limited to about 100 GHz.

According to the same formula, the Brillouin and thus the detection frequency can be increased by decreasing the probe wavelength. So we first use an UV probe wavelength in order to measure the high-frequency content of the strain pulse emitted from the QD. In Fig. 2(a), we present a zoom-in of the echo detected either in blue (450 nm) or in medium UV (266 nm). The echo detected at 266 nm is found significantly shorter than at 450 nm and the oscillating part has almost disappeared. This is related to the strong optical absorption of the UV light in InP: The extinction coefficient k in InP is 0.7 at 450 nm and 2.8 at 266 nm.[15]

In Fig. 2(b) we compare the spectrum of both echoes. First one can notice a higher central frequency of the pulse detected with an UV probe, as expected. At 450 nm (resp. 266 nm), the pulse is centered at 100 GHz (resp. 150 GHz). One should remark that the magnitude of the echo detected at 150 GHz is still strong which confirms that the frequency content was limited by detection and not by the strain pulse

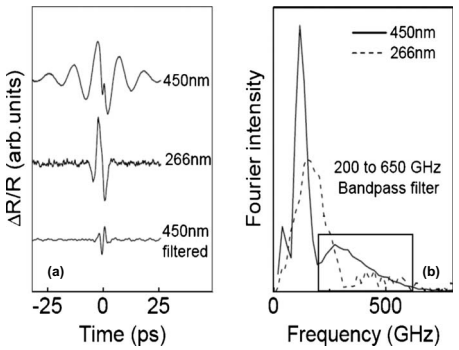

FIG. 2. (a) Shape comparison between the experimental echo detected at 450 and 266 nm. The last structure results from the application on the 450 nm experimental echo of a 200–650 GHz band-pass filter. (b) Fourier transform of the experimental echoes.

itself. The difference between echo durations in the time domain is manifested in the Fourier space on the spectrum width. The strong absorption of the UV light offers a larger bandwidth detection. As shown in Fig. 2(b), at 266 nm, we can detect some acoustic components up to 300 GHz.

A frequency increase is observed (from 100 to 150 GHz), but the detected value is still far from terahertz. Looking carefully at the spectrum of the echo detected at 450 nm, one remarks that it is composed of two different contributions, well separated in the frequency domain. Each of these is related to a specific part in the time domain. The low-frequency peak (up to 200 GHz) corresponds to the Brillouin oscillations. The high-frequency bump, from 200 GHz to 650 GHz, is related to the fast structure visible at the center of the echo. This is more evident in Fig. 2(a) where we compare the raw echo and the filtered echo (200–650 GHz band-pass filter). On the filtered signal, Brillouin oscillations have disappeared and the oscillating echo is replaced by a very short structure. This part is already visible on the raw echo as a small accident at the center of the echo. This first proves that some high-frequency components are already detected using a blue probe. Second it shows that the phonon wave packet emitted from the QD layer contains up to 650 GHz components.

To go further and especially to understand the appearance of such a high-frequency structure, we need to have a better insight in the photoelastic mechanism. The change in reflectivity caused by the strain is given by[16]

$$\Delta R(t) = \int_{z=0}^{+\infty} f(z)\,\eta(z,t)dz, \tag{1}$$

where $\eta(z,t)$ is the strain at the depth z at delay t and f is the sensitivity function which is defined by

$$f(z) = f_0\left[\frac{\partial n}{\partial \eta}\sin\left(\frac{4\pi nz}{\lambda} - \phi\right) + \frac{\partial k}{\partial \eta}\cos\left(\frac{4\pi nz}{\lambda} - \phi\right)\right]e^{-4\pi kz/\lambda}, \tag{2}$$

with

$$f_0 = \frac{16\pi[n2(n2+k2-1)2+k2(n2+k2+1)2]^{1/2}}{\lambda[(n+1)2+k2]2}, \quad (3)$$

and

$$\tan\phi = \frac{k(n2+k2+1)}{n(n2+k2-1)}. \quad (4)$$

In these expressions, λ is the probe wavelength in vacuum, n is the refractive index, k is the extinction coefficient, and $\partial n/\partial\eta$ and $\partial k/\partial\eta$ are the photoelastic constants.

Equation (2) offers a simple way of identifying the two frequency components of the echo. The sensitivity function is composed of oscillating functions (sine and cosine) exponentially damped by the optical absorption. In case of a probe wavelength for which the absorption length is long, the convolution of the oscillating functions with a strain pulse leads to Brillouin oscillations. This is the origin of the low-frequency part of the spectrum centered around the Brillouin frequency $(2nv/\lambda)$.

Second we show that depending on the photoelastic constants, the sensitivity function can experience a discontinuity at $z=0$ which is responsible of the detection of the high-frequency component. To clarify this last point, we examine the shape of the sensitivity function close to $z=0$ for different sets of photoelastic constants. In Eq. (1), one calculates the integral between f and η on the half space $z \geq 0$. In that case η is composed of two counterpropagating pulses to describe the total acoustic reflection at the free surface. The incoming and returning pulses have opposite signs due to the acoustic mismatch between air and InP. It is straightforward to see that Eq. (1) can be rewritten as an integral over the full space, using a single strain pulse but using an *odd* sensitivity function defined by Eq. (2) for $z \geq 0$ and for each z verifying $f(-z)=-f(z)$. The odd character of the sensitivity function is introduced to reproduce the sign change of the strain at the free surface.

Figure 3(a) compares the sensitivity function obtained using two different couples of photoelastic constants. According to the previous calculation, f experiences a $2f(0)$ discontinuity at the free surface $(z=0)$. Once the optical properties are defined, ϕ is fixed and the discontinuity is governed by the photoelastic constants. Such a discontinuity in the sensitivity function, leads to a sudden change at the echo center similarly to what is shown in Fig. 2(a). In the frequency domain a sudden change means high-frequency components. In Fig. 3(b), we compare the high-frequency content of the echo detected by the two sensitivity functions. We use a δ-function as a strain so that we can focus on detection effects. As shown, the discontinuity created by the photoelastic constants choice greatly improves the detection of high frequency.

Experimentally, we cannot adjust the photoelastic constants. But they are sensitive to the probe wavelength especially in the vicinity of an electronic interband transition.[17,18] So strong changes in the echo spectrum are expected when tuning the probe around such a transition. Here we take advantage of the InP E_1 transition, located at 394 nm.[10] We performed experiments with a probe wavelength comprise between 380 and 400 nm. The Fourier transform of the corresponding echoes is represented in Fig. 3(c). Depending on which side of the transition we tune the probe, the high-frequency bump appears or not, confirming that the photoelastic constants can be significantly changed in the vicinity of the transition.

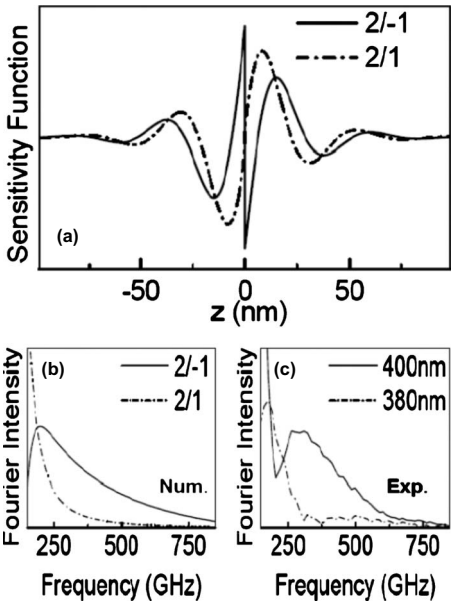

FIG. 3. (a) Sensitivity function calculated with InP properties at 400 nm for two sets of photoelastic constants $(\partial n/\partial\eta;\partial k/\partial\eta)$: (2;1) and (2;−1). (b) Fourier transform of the theoretical signal obtained using a δ-function as a strain pulse. (c) Fourier transform of the experimental signal measured at 380 and 400 nm.

From the theoretical analysis we thus conclude that by tuning the probe wavelength around an interband transition one can change the photoelastic constants and doing that one can find a wavelength at which the sensitivity function experiences a discontinuity at the free surface which permits the detection of the high-frequency part of the strain pulse. In case of InP we found that 390 nm is the wavelength at which the sensitivity function offers the highest frequency photoelastic detection.

Using the best wavelength conditions to detect high-frequency components of the strain pulse we come back to our problematic of frequency content of the strain pulse emitted from QD. Another main limitation in the detection of terahertz acoustic pulse is the attenuation of longitudinal phonons which is roughly proportional to the squared frequency. In order to minimize the attenuation, we choose to work on a sample with a 100 nm thick InP cap. The echo obtained at 390 nm on the sample is shown in Fig. 4(a). The thinner cap compare to the previous samples is manifest by the shorter time of arrival of the echo. The Fourier transform visible in Fig. 4(b) presents a two components spectrum as in the previous sample but shifted toward higher frequency. We clearly see that there is component in the terahertz range. As the experiment was performed at room temperature at which the phonon attenuation is still strong, the amplitude of the terahertz part of the strain emitted from the QD layer is much stronger than shown here. Working at low temperature could help the detection of even higher frequency.

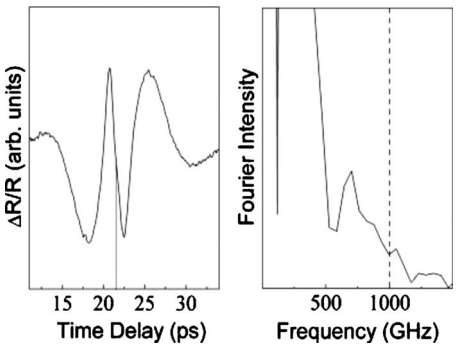

FIG. 4. (a) Experimental echo detected at the surface of the sample with a 100-nm-thick cap at 390 nm. (b) Fourier transform of the experimental signal.

One of the remaining question is the exact emitting zone, whether it is the QD layer itself or the wetting layer (WL). By performing experiments at various places on the sample, we observed a shift of the high-frequency contribution that can reach 150 GHz. The high-frequency part is especially sensitive to the size of the emitting zone. Using a numerical modeling we estimate that a 2-nm-height variation is needed to reproduce a 150 GHz shift. In epitaxial QD system, the fluctuations of the WL thickness are expected to be less than 1 ML. On the contrary, such fluctuations of the QD height are currently observed.[19] Thus this observation confirms that QD layer plays a direct role in the strain pulse emission.

We have reported on the generation of terahertz longitudinal-acoustic waves from QD using femtosecond light pulses. Frequencies above 1 THz have been detected. We explain the detection process by a significant variation of the photoelastic constants in the vicinity of an interband transition. Thanks to the high-frequency component and to its sensitivity to size fluctuations, we confirm the role played by the QD in the acoustic emission. That illustrates the main interest in using THz acoustics for probing nanoscale objects. The model developed here can be useful to predict for any material the wavelength at which the highest acoustic frequency can be detected in ultrafast acoustics. This can, for example, be applied to hypersound attenuation measurement in thin films.

The authors want to thank Simon Ayrinhac for his helpful contribution to the third-harmonic generator.

*arnaud.devos@isen.fr

[1] P. Hawker, A. J. Kent, and M. Henini, Physica B **263-264**, 514 (1999).
[2] K.-H. Lin, C.-M. Lai, C.-C. Pan, J.-I. Chyi, J.-W. Shi, S.-Z. Sun, C.-F. Chang, and C.-K. Sun, Nat. Nanotechnol. **2**, 704 (2007).
[3] B. Perrin, B. Bonello, J.-C. Jeannet, and E. Romatet, Physica B **219-220**, 681 (1996).
[4] A. Devos, M. Foret, S. Ayrinhac, P. Emery, and B. Rufflé, Phys. Rev. B **77**, 100201 (2008).
[5] P. M. Walker, A. J. Kent, M. Henini, B. A. Glavin, V. A. Kochelap, and T. L. Linnik, Phys. Rev. B **79**, 245313 (2009).
[6] A. Huynh, N. D. Lanzillotti-Kimura, B. Jusserand, B. Perrin, A. Fainstein, M. F. Pascual-Winter, E. Peronne, and A. Lemaître, Phys. Rev. Lett. **97**, 115502 (2006).
[7] A. Bartels, T. Dekorsy, H. Kurz, and K. Köhler, Phys. Rev. Lett. **82**, 1044 (1999).
[8] C.-K. Sun, J.-C. Liang, and X.-Y. Yu, Phys. Rev. Lett. **84**, 179 (2000).
[9] A. Devos, F. Poinsotte, J. Groenen, O. Dehaese, N. Bertru, and A. Ponchet, Phys. Rev. Lett. **98**, 207402 (2007).
[10] O. Madelung, *Semiconductors Groupe IV Elements and III-V Compounds* (Springer-Verlag, Berlin, 1991).
[11] C. Paranthoen, N. Bertru, O. Dehaese, A. L. Corre, S. Loualiche, B. Lambert, and G. Patriarche, Appl. Phys. Lett. **78**, 1751 (2001).
[12] Y. R. Shen, *The Principles of Nonlinear Optics* (Wiley-Interscience, New York, 1984).
[13] V. Petrov, F. Rotermund, F. Noack, J. Ringling, O. Kittelmann, and R. Komatsu, IEEE J. Sel. Top. Quantum Electron. **5**, 1532 (1999).
[14] C. Thomsen, H. T. Grahn, J. Tauc, and H. J. Maris, Opt. Commun. **60**, 55 (1986).
[15] E. D. Palik, *Handbook of Optical Constants of Solids* (Academic Press, London, 1985).
[16] C. Thomsen, H. T. Grahn, H. J. Maris, and J. Tauc, Phys. Rev. B **34**, 4129 (1986).
[17] A. Devos and C. Lerouge, Phys. Rev. Lett. **86**, 2669 (2001).
[18] A. Devos and A. Le Louarn, Phys. Rev. B **68**, 045405 (2003).
[19] B. Joyce, P. Kelires, A. Naumovets, and D. Vvedensky, *Quantum Dots: Fundamentals, Applications and Frontiers* (Springer, Berlin, 2005).